Macromolecules

ARTICLE

pubs.acs.org/Macromolecules

Elasticity of Rigidly Cross-Linked Networks of Athermal Filaments

Goran Žagar,* Patrick R. Onck, and Erik Van der Giessen*

Micromechanics of Materials, Zernike Institute for Advanced Materials, University of Groningen, Nijenborgh 4, 9747 AG Groningen, The Netherlands

Supporting Information

ABSTRACT: Actin filaments assemble into network-like structures and play an important role in various cellular mechanical processes. It is known that the response of actin networks cross-linked by stiff proteins is characterized by two distinct regimes: (i) a linear stress−strain response for small deformations and (ii) a power law relation between elastic shear modulus and stress with an exponent 3/2 for large deformations. If the response is interpreted by the entropic single filament model, this hardening is attributed to the reduction of the thermal filament fluctuations as the filaments undergo affine stretching. By contrast, here we numerically study the elastic properties of a discrete, fully three-dimensional model for an isotropic filamentous networks, where athermal filaments of finite length are interconnected by rigid cross-links. By analyzing the network microstructure, the network connectivity is quantified in terms of the ratio of the mean filament length and the mean cross-linking distance along the filament. We derive a scaling relation for the initial network shear modulus—i.e., regime i—as a function of the network connectivity. When sheared to large strains, the simulated networks exhibit nonlinear strain hardening characterized by a 3/2 power law—regime ii. The origin of the strain hardening is shown to be associated now with the stretching of percolating and nearly fully extended stress paths in the network. In addition, we show that the strain at the onset of the strain hardening regime only depends on the network connectivity.

1. INTRODUCTION

The mechanical properties of living cells are related to the organized structure of filamentous proteins in the cytoskeleton. Filaments polymerized from globular actin (F-actins), being the major cytosleketal constituent, are involved in the formation of the complex network-like structures that play a key role in maintaining the cells mechanical stability and shape.[1] In order to circumvent the cytoskeleton complexity, most investigations of mechanical properties of F-actin networks are carried out on *in vitro* reconstituted actin gels, which already exhibit a rich mechanical behavior.[2,3]

While *in vitro* F-actins alone entangle in a weak gel, low to moderate concentrations of actin binding proteins are capable of cross-linking F-actins into stronger isotropic networks of individual filaments. At moderate to high concentrations, many of the cross-linking proteins tend to bundle the F-actins.[3] The mechanical response of cross-linked networks depends sensitively on the structure of the cross-linking proteins.[4] In the case of "stiff" cross-linking proteins, such as scruin[5] or heavy meromyosin,[6] the mechanical behavior of the network originates mainly from the F-actins themselves.

Numerous rheological experiments on F-actin networks have shown that the elastic stress−strain behavior is linear at small strains, and is followed by highly nonlinear strain hardening at large strains.[6,7] Remarkably, the hardening is characterized by a power law dependence of the elastic shear modulus on the macroscopic stress with exponent 3/2.[5,8] Recently, the same power law dependence has been observed in ionically cross-linked networks of intermediate filaments,[9,10] which suggests that this scaling may be generic for networks, at least within a range of filament properties.

A continuum network model based on the physics of free-standing single filaments[11,12] associates the 3/2 exponent in the strain hardening scaling law to the entropy of the thermally fluctuating filaments. In this view, the network is considered as a collection of randomly oriented thermal semiflexible polymers that are deforming by affine stretching. However, the assumption that the microscopic deformation of the network is affine is rather controversial, primarily because of numerical studies that clearly show strong nonaffine trends.[13−16] In addition, once the filament is cross-linked into the network, its thermal fluctuations are expected to be somewhat suppressed due to constrains imposed by the cross-links,[17] especially when the length of sections between cross-links is small.[6,9]

Recently, Onck et al.,[15] based on 2D network simulations, proposed an alternative mechanism for strain hardening in filamentous networks. In this view, nonaffinity and network microstructure play a key role in mediating the transition from a regime dominated by the filament bending stiffness at small strains to a large strain regime dominated by the axial stiffness of filaments. Moreover, subsequent simulations of 3D networks hinted that the network connectivity, whether simply considered as a static property of the microstructure[16] or as a dynamic strain-driven remodeling factor,[18] plays an important role for the network response.

Since individual F-actins within the network are too thin to be observed experimentally, many details about the role of the microstructure for the network response are still missing or poorly understood. In this paper we will investigate the role of the microstructure on the stress−strain response of discrete 3D random networks of cross-linked and unbundled filaments using the numerical approach previously reported by Huisman et al.[16]

Received: June 3, 2011
Revised: July 22, 2011
Published: August 05, 2011

Isotropic and homogeneous random networks will be generated from filaments that are athermal and finite in length. The cross-links in the network are allowed to connect only a single filament pair and will be considered as permanent and rigid. Thus, there is no relative motion between the two filaments at the cross-linking site.

The paper is organized as follows. In section 2, we will analyze the topology of the network microstructure and adopt a convenient measure for network connectivity. In section 3, we will empirically derive the scaling relation for the initial network shear modulus. This, and the subsequent analysis of the large strain network behavior carried out in section 4, will highlight the importance of the microstructure for the network mechanical behavior. Finally, in section 5, we summarize the main results and draw conclusions.

2. NETWORK TOPOLOGY

While the generation of a random network in two dimensions is rather straightforward, this is not so in 3D and a few methods have been proposed in the literature to numerically construct representative volume elements (RVE) of homogeneous isotropic networks of cross-linked filaments.[14,16,19] Here we analyze random networks that self-assemble by means of a dynamics procedure proposed by Huisman et al.[16] A system of filaments of length l_0 is contained in a periodic box of size W^3 and set into motion by a weak $1/r^2$ attractive force field. The number of filaments in the box, n_f, is determined by the concentration of the filamentous constituent defined as $c_f = \rho_f(t/2)^2\pi n_f l_0/W^3$, where ρ_f and t are filament density and diameter, respectively. Initially, randomly positioned and oriented straight filaments are discretized into 3D beam finite elements that can stretch, bend and twist. The filament motion is assumed to take place in a viscous fluid environment, giving rise to hydrodynamic drag, and for numerical convenience, we also consider internal damping in the filaments. If two filaments approach each other within a certain threshold distance, they become rigidly connected by a permanent cross-link. The multiple cross-linking of filaments results in filaments that are partitioned into sections. The generation process is stopped once the desired mean length of filament sections, l_c, is reached. Generally, the dynamics procedure generates internally stressed networks, but this prestress is neglected subsequently. The force field parameters are tuned to avoid the formation of filament bundles. For given material parameters of the filaments, the microstructure of the generated network can be controlled by varying the total concentration of filaments c_f, the initial filament length l_0 and the mean filament section length l_c. Any set of random RVE realizations with the same network microstructure is therefore associated with a triplet (c_f, l_0, l_c). Detailed molecular dynamics (MD) simulations of the assembly of cross-linked actin networks by Kim et al.[19] have shown that the length of the filaments in a network is distributed. Despite the fact that in our simulations all filaments have the same initial length l_0, the microstructure of the networks generated by the dynamics procedure[16] is comparable with that generated by the MD simulations[19] in the sense that the filament section lengths have a similar exponentially decreasing distribution.

The part of the RVE microstructure that controls its mechanical behavior is a percolating supportive subnetwork that excludes filament dangling ends and isolated (disconnected) filament clusters. A dangling end is defined as a filament section that is free on one end (see Figure 1). An isolated filament cluster is

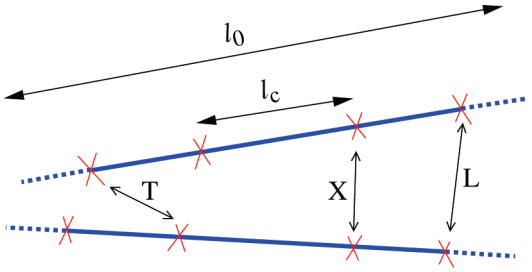

Figure 1. Two filaments of length l_0 making an L, T, or X cross-link. The outer−outer joining of the cross-linking sites of two filaments forms L cross-links, while the outer−inner or inner−inner joining forms T or X cross-links, respectively. The average cross-link separation along the filament, i.e. the mean filament section length, is l_c. Dangling ends are drawn dashed.

defined as a finite size cluster of filament sections that is not connected to the subnetwork. Because dangling ends and isolated filament clusters cannot deform under mechanical load (they only experience rigid body motions), they are irrelevant for the mechanical behavior. The removal of mechanically irrelevant parts from the network, especially the dangling ends, leads to an important morphological characteristic of supportive subnetwork, namely that the cross-link coordination in the network becomes distributed. We distinguish 4-coordinated "X"-cross-links, 3-coordinated "T"-cross-links, and 2-coordinated "L"-cross-links.

The topology of a network (from now on, we just use "network" for the supportive subnetwork) is fully defined in terms of five parameters: the number of sections n_s, the number of cross-links n_{cl} and the number of L-, T-, and X- coordinated cross-links, i.e. n_L, n_T and n_X, respectively. These five topological parameters are related by two "conservation" equations:

$$1 = \tilde{n}_L + \tilde{n}_T + \tilde{n}_X \tag{1a}$$

$$\tilde{n}_s = \frac{1}{2}(2\tilde{n}_L + 3\tilde{n}_T + 4\tilde{n}_X) \tag{1b}$$

where $\tilde{n}_s = n_s/n_{cl}$ and $\tilde{n}_L$, $\tilde{n}_T$, and $\tilde{n}_X$ are the fractions of L-, T-, and X-cross-links, respectively.

The fractions $\tilde{n}_L$, $\tilde{n}_T$ and $\tilde{n}_X$ represent the probabilities of finding a cross-link of either L-, T-, or X-type, which is equivalent to the probability that two filaments actually make a cross-link of that type. Since a filament with mean length l_0 comprising sections with mean length l_c contains $(l_0 - l_c)/l_c$ cross-linking sites (see Figure 1), the probability of finding a cross-linking site along the filament is $1/(\tilde{l}_0 - 1)$, with $\tilde{l}_0 = l_0/l_c$. The probability of finding any of the two outer cross-linking sites of a filament is therefore $2/(\tilde{l}_0 - 1)$, while the probability of finding any of the inner sites is $((\tilde{l}_0 - 3)/(\tilde{l}_0 - 1))$. Since the joining of the outer sites of two filaments corresponds to an L cross-link, the joining of an inner and an outer site to a T cross-link and the joining of two inner sites to an X cross-link, the fractions $\tilde{n}_L$, $\tilde{n}_T$, and $\tilde{n}_X$ can be expressed as

$$\tilde{n}_L = \frac{4}{(\tilde{l}_0 - 1)^2}, \quad \tilde{n}_T = 4\frac{\tilde{l}_0 - 3}{(\tilde{l}_0 - 1)^2},$$
$$\tilde{n}_X = \frac{(\tilde{l}_0 - 3)^2}{(\tilde{l}_0 - 1)^2} \tag{2}$$

dx.doi.org/10.1021/ma201257v |*Macromolecules* 2011, 44, 7026–7033

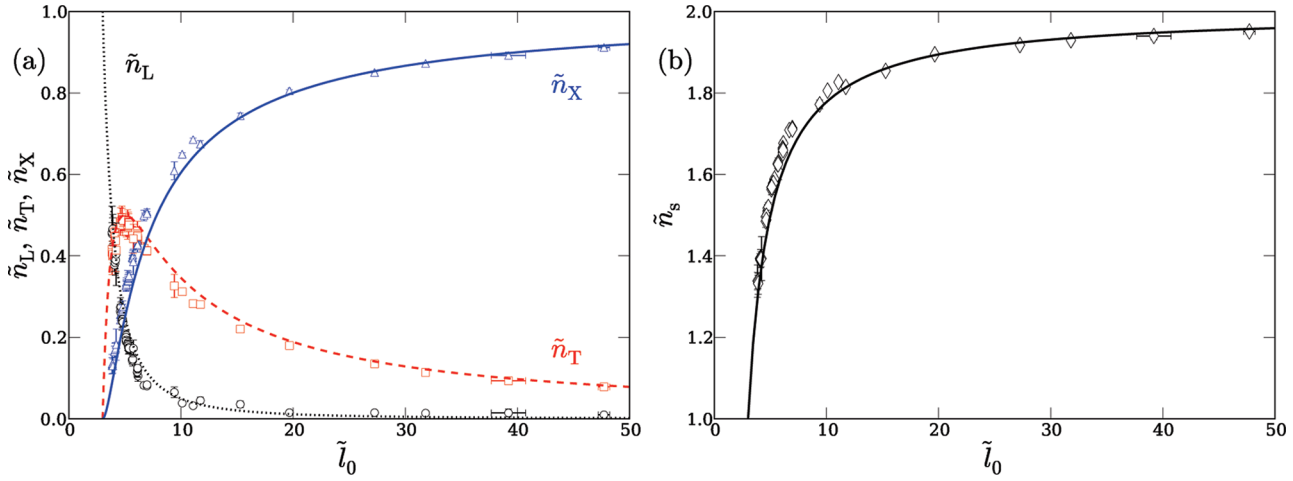

Figure 2. Topology of networks generated with the filament dynamics procedure:[16] (a) $\tilde{n}_L$ (black circle, dotted line), $\tilde{n}_T$ (red square, dashed line), and $\tilde{n}_X$ (blue triangle, solid line) as a function of $\tilde{l}_0$. The lines are predictions according to eq 2. (b) $\tilde{n}_s$ as a function of $\tilde{l}_0$. The solid line is the prediction according to eq 3. Each data point corresponds to the mean value of seven to ten random realizations generated for a triplet (c_f, l_0, l_c) where c_f is 0.8, 1, 1.5, 2, 2.5, or 4 mg/mL; l_0 is 1.5, 1.8, 2.1, 3, 4, 5, 6, 8, 10, or 20 μm, and l_c ranges from ≈0.02 l_0 to ≈0.25 l_0. Depending on c_f and l_0 and for the box size W = 2.5 μm[16] the number of filaments n_f ranges from ≈50 to ≈500. The filament diameter and density parameters are taken to represent filamentous actin: $t \approx 7$ nm and $\rho_f \approx 1300$ mg/mL.[20]

Combination of eq 2 and eq 1b then gives

$$\tilde{n}_s = 2\frac{\tilde{l}_0 - 2}{\tilde{l}_0 - 1} \tag{3}$$

Thus, it follows that the topology of our random networks depends only on a single parameter: the ratio of the mean filament length l_0 and the mean filament section length l_c through $\tilde{l}_0 = l_0/l_c$. The topology predicted by eq 2 and eq 3 agrees very well with the data extracted from a large set of generated networks, as shown in Figure 2. The lower limit of $\tilde{n}_s$ at small $\tilde{l}_0$ corresponds to an L-only coordinated network ($\tilde{n}_L = \tilde{n}_s = 1$) formed by a percolation of filament sections with one section per filament. The L-only coordinated network sets the upper bound for the maximum mean filament section length to $l_c = l_0/3$, with the two remaining sections being the dangling ends. The other topological limit is the X-only network ($\tilde{n}_X = 1$, $\tilde{n}_s = 2$), where each cross-link connects four sections and is reached in the limit $\tilde{l}_0 \to \infty$.

The eq 2 and eq 3 suggest several equivalent ways of quantifying the network connectivity. Since the fraction of X cross-links $\tilde{n}_X$ (see Figure 2) is found to be the slowest varying function of $\tilde{l}_0$ over the entire connectivity range, it is the most convenient measure. Obviously, $\tilde{n}_X = 0$ corresponds to an L-only network with connectivity 2, while $\tilde{n}_X = 1$ corresponds to an X-only network with connectivity 4.

3. SMALL STRAIN NETWORK RESPONSE

Besides topology, the mechanical properties of a network are determined by the constituent filaments between the cross-links. When the persistence length l_p of the filaments is much larger than the average length of the sections, i.e. $l_p \gg l_c$, the sections can be considered as being straight. The ratio of the filament bending stiffness κ_f and stretching stiffness μ_f denotes the length scale $l_b = (\kappa_f/\mu_f)^{1/2}$.[21] In addition, bending dominated structures are expected for a mean cross-link coordination ≈6 and below.[22] A network with straight sections and $l_c > l_b$ therefore, is a bending dominated structure similar to an open cell foam. Thus, the small-strain elastic shear modulus G_0 should scale as $G_0 \propto \kappa_f/l_c^4(l_c/\xi)^2$,[23,24] with ξ being the mesh size. [Note that for a foam, $l_c \approx \xi$ and $\xi \propto 1/(c_f)^{1/2}$, so the scaling of the initial modulus with filament concentration is quadratic, $G_0 \propto c_f^2$, which is close to the scaling $G_0 \propto c_f^{11/5}$ proposed by MacKintosh et al.][11] By extending this scaling relation with an appropriate function f of the set of topological parameters $\mathcal{T}$, all the effects arising from the network topology can be accounted for in $G_0 \propto \kappa_f/l_c^4(l_c/\xi)^2 f(\mathcal{T})$. The identification of the topological function $f(\mathcal{T})$ has been addressed in detail elsewhere;[25] here, we briefly summarize the results.

Sets of seven to ten random network realizations were generated with the dynamics procedure[16] for a range of initial filament concentrations $c_f \approx 0.8, ..., 4$ mg/mL, lengths $l_0 \approx 1.5, ...,$ 20 μm and $l_c \approx 0.02l_0, ..., 0.25l_0$. The fraction of X cross-links of the generated networks covered the range of connectivities $\tilde{n}_X \approx$ 0.10, ..., 0.92. Each generated network was discretized by finite elements and subjected to simple shear.[16] The ensemble average initial elastic shear modulus, G_0, was calculated by averaging the initial responses of the set realizations. The material parameters used for the filament elements are based on the parameters common to filamentous actin: axial stiffness $\mu_f = 4 \times 10^{-8}$ N,[26] bending stiffness $\kappa_f = 6.75 \times 10^{-26}$ N m^2,[27] while the torsional stiffness is taken to be equal to the bending stiffness. The nondimensional parameters used for studying the system at small strains are the normalized initial elastic shear modulus $G_0 l_c^4/\kappa_f$, the geometrical parameter l_c/ξ and the topological parameter $\tilde{n}_X$.

The contribution of the network topology to the initial network shear modulus G_0 is found to be 2-fold: first, compared to the topology-free scaling law $G_0 \propto \kappa_f/l_c^4(l_c/\xi)^2$ there is an extra dependence of G_0 on the ratio l_c/ξ. Then, as the inset of Figure 3 shows, if $G_0(l_c^4/\kappa_f)(l_c/\xi)^{-3}$ is plotted against $\tilde{n}_X$, the data points follow the trend set by a power law with exponent 2.5, so that $G_0 \propto \kappa_f/l_c^4(l_c/\xi)^3(\tilde{n}_X)^{2.5}$. By construction, the scaling relation for G_0 tends to underestimate the G_0 at very small network connectivities ($\tilde{n}_X < 0.1$), as it predicts $G_0 \to 0$ for

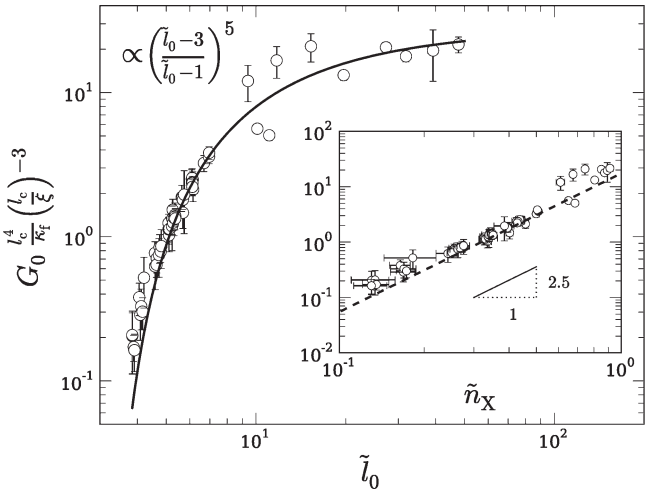

Figure 3. Normalized initial elastic shear network modulus G_0 as a function of $\tilde{l}_0$. The solid line is a fit of the function $A[(\tilde{l}_0-3)/(\tilde{l}_0-1)]^5$, with A being the proportionality constant. Inset: the normalized initial elastic shear network modulus G_0 as a function of $\tilde{n}_X$. The dashed line is a power law fit in $\tilde{n}_X$ with exponent 2.5. The data sets used are the same as in Figure 2.

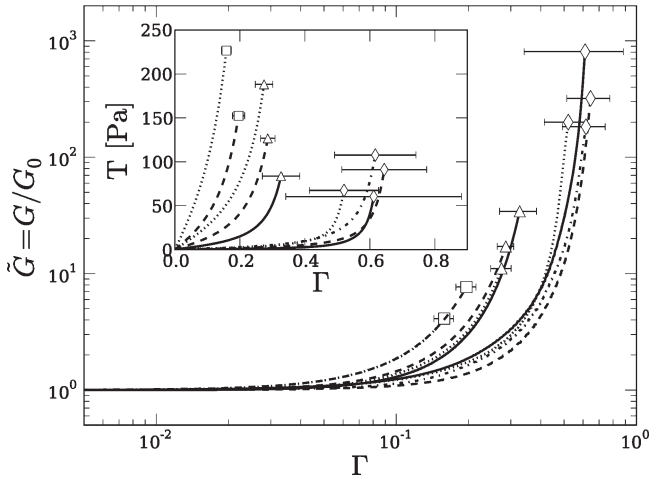

Figure 4. Normalized elastic shear modulus $\tilde{G} = G/G_0$ as a function of macroscopic shear strain Γ for generated network sets with connectivity $\tilde{n}_X$: ≈ 0.17 (◇), ≈ 0.4 (△), and ≈0.5 (□) and various values of the filament concentration c_f in mg/mL: 1 (solid); 1.5 (dashed); 2 (dash-dotted); 2.5 (dotted). Inset: Corresponding macroscopic stress−strain curves.

vanishingly small $\tilde{n}_X$, despite the fact that G_0 will have a small nonzero value at the geometric percolation limit. By substituting $\tilde{n}_X$ according to eq 2, the scaling relation can be rewritten as

$$G_0 \propto \frac{\kappa_f}{{l_c}^4}\left(\frac{l_c}{\xi}\right)^3\left(\frac{\tilde{l}_0-3}{\tilde{l}_0-1}\right)^5 \tag{4}$$

Indeed, if now $G_0({l_c}^4/\kappa_f)(l_c/\xi)^{-3}$ is plotted against $\tilde{l}_0$ (main graph in Figure 3), all data points follow the trend set by the proportionality $\propto [(\tilde{l}_0-3)/(\tilde{l}_0-1)]^5$ (solid line).

4. LARGE STRAIN NETWORK RESPONSE

The nonlinearity of the network response is commonly demonstrated by plotting the instantaneous shear modulus normalized by the initial stiffness, $\tilde{G} = G/G_0$, versus the macroscopic shear strain Γ or the macroscopic shear stress T. If the onset of the nonlinear dependence of $\tilde{G}$ on strain Γ or stress T is denoted by the "critical strain" Γ_c or "critical stress" T_c respectively, the plot of $\tilde{G}$ against Γ/Γ_c or T/T_c often collapses the network response onto a master curve, as seen in many experiments.[5,8,10] The master curves, obtained in this way, are an indication of universal network behavior. Conversely, the nonlinear behavior of a specific network can be predicted from these master curves if G_0, Γ_c, and/or T_c are known.

The strain-dependent response for a 3D periodic network is obtained from a quasi-static finite element simulation (simple shear with prescribed macroscopic strain) suitable for large deformations (updated Lagrangian).[16] The ensemble average macroscopic stress−strain response T(Γ) of a set of seven to ten random realizations generated for the triplet (c_f, l_0, l_c), is obtained by averaging the realization responses at a constant stress level. The average network shear modulus G as a function of strain Γ follows from the stress−strain response T(Γ), i.e. $G = \partial T/\partial\Gamma$. All large strain simulations here are limited to the strain level at which the axial stress in a filament element exceeds the actin filament strength of ≈300 pN.[26]

The scaling relation in eq 4 reveals that the initial network response G_0 is a function of κ_f, ξ, l_c and l_0 (or the function $\tilde{n}_X(\tilde{l}_0)$). At large strains, the network modulus G might also depend on those parameters so that after scaling with G_0, some of these dependencies in $\tilde{G}$ might drop out, fully or partially. Because of normalization with G_0, the scaled modulus $\tilde{G}$ obviously becomes independent of the filament bending stiffness κ_f. Since the mesh size is uniquely defined by the total concentration of filaments in the RVE, i.e., $\xi \propto 1/(c_f)^{1/2}$, we hypothesize that $\tilde{G}$ does not depend on ξ in another way then contained in G_0 through eq 4. To confirm this, Figure 4 shows the scaled network modulus as a function of strain for $\tilde{n}_X \approx 0.17$ (diamond), 0.4 (triangle), and 0.5 (square) and for different values of c_f. As clearly seen from Figure 4, the responses $\tilde{G}(\Gamma)$ for constant $\tilde{n}_X$ and different c_f are indistinguishable within the error bars, thus confirming our hypothesis. Accounting for all scaled out parameters, $\tilde{G}(\Gamma)$ depends only on the network connectivity $\tilde{n}_X(\tilde{l}_0)$.

Figure 5 shows large strain responses for several network sets. Initially, the network response to shear is linear, up to the critical stress T_c or critical strain Γ_c, after which the response becomes highly nonlinear. If the normalized network shear modulus $\tilde{G}$ is plotted against the macroscopic stress T (see inset, Figure 5b), we find that the nonlinear part is characterized by a power law dependence with exponent 3/2, i.e. $\tilde{G} \propto T^{3/2}$. Subsequently, from the inset of Figure 5b, the critical stress T_c for each data set is determined as the stress at the onset of the nonlinearity. After this, as shown in the main graph of Figure 5b, normalization of stress with the extracted T_c values collapses all the data onto a single master curve. This master curve can be described by

$$\tilde{G} = \begin{cases} 1, & T/T_c < 1 \\ 1 + a(T/T_c - 1)^{3/2}, & T/T_c \geq 1 \end{cases} \tag{5}$$

with a universal constant a, that for the material parameters used in this work, is found to be $a = 0.1$. The corresponding two master curves, namely Γ/Γ_c vs $\tilde{G}$ and Γ/Γ_c vs T/T_c, can be found by rescaling the strain axis with the corresponding critical strain Γ_c

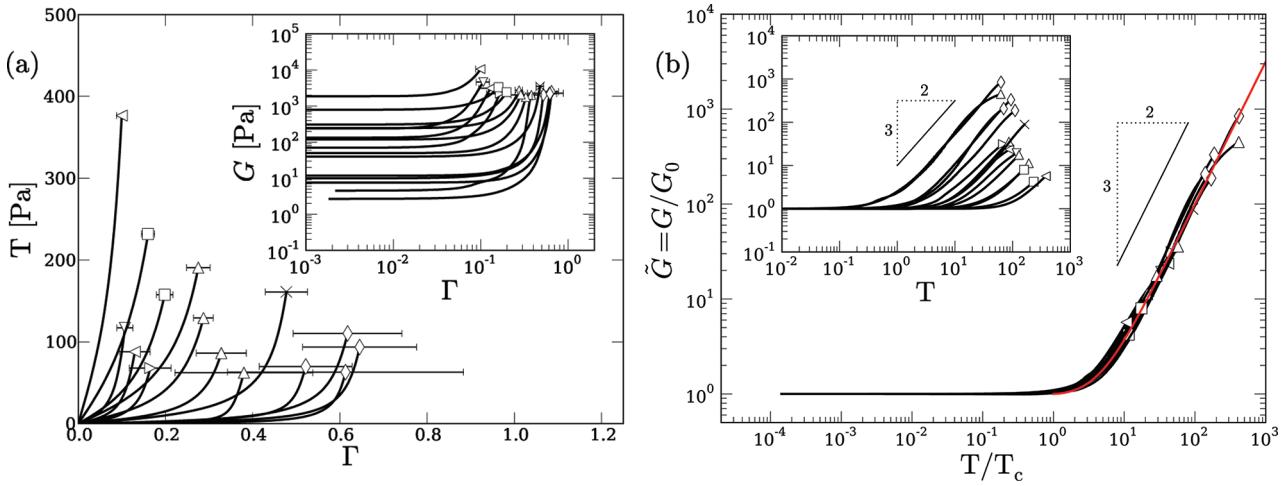

Figure 5. Averaged nonlinear network behavior at large strain. (a) Macroscopic shear stress T as a function of macroscopic shear strain Γ. Inset: Corresponding elastic network shear modulus $G = \partial T/\partial \Gamma$. (b) After scaling the network modulus G by G_0 and stress T by critical stress T_c all data (inset) collapse onto a master curve. The master curve (red) is represented by the function $\tilde{G}$ in eq 5 with $a = 0.1$. The symbols correspond to the network connectivity $\tilde{n}_X$: ≈ 0.17 (◇), ≈ 0.25 (×), ≈ 0.4 (△), ≈ 0.5 (□), ≈ 0.6 (triangle pointing right), ≈ 0.65 (triangle pointing left), and ≈ 0.75 (▽).

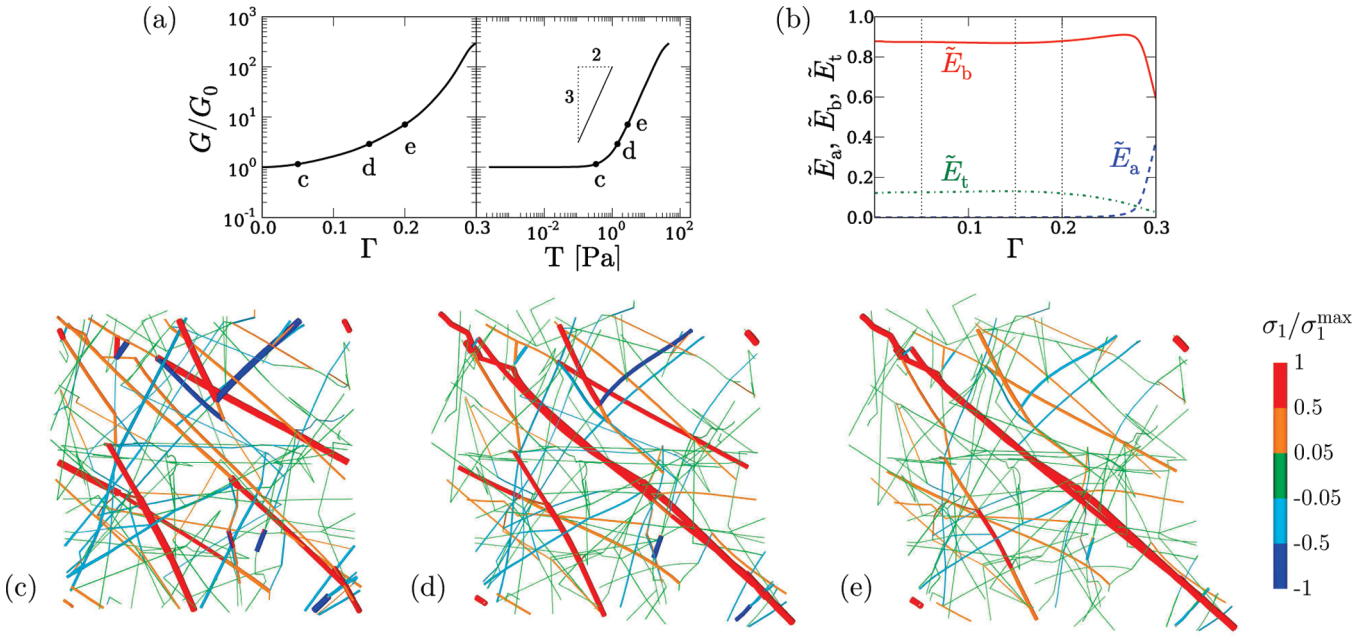

Figure 6. (a) Large strain response of a network realization generated with connectivity $\tilde{n}_X$: ≈ 0.34. (b) Relative axial $\tilde{E}_a$ (dashed), bending $\tilde{E}_b$ (solid), and torsional $\tilde{E}_t$ (dash-dotted) energy in the network as a function of shear. The energies are normalized by the total strain energy $E_a + E_b + E_t$. (c−e) Axial stress map of the corresponding network microstructure at a shear strain Γ: ≈ 0.05, ≈ 0.15, and ≈0.20, as indicated by the symbols in the graph in panel a and vertical lines in panel b, respectively. The color and the thickness in the maps indicate a level of element axial stress relative to the maximum element axial stress, σ_1/σ_1^{max}.

obtained from the corresponding T−Γ curve shown in Figure 5a, i.e. $T_c = T(\Gamma_c)$. Expressions for the other two master curves are derived in the Supporting Information.

To understand the origin of network stiffening, it is instructive to look at the microstructure of the network as it is sheared. Figure 6c−e shows a view through a deformed network with connectivity $\tilde{n}_X \approx 0.34$ and a superimposed color map of the normalized axial stress. Three snapshots near the critical point are shown. The initial linear network response, captured by eq 4, is governed by bending and reorientation of the network sections.[15,16] At small shear strains (Figure 6c), a few axially stressed sections are present, separated from each other by low stressed network regions. As the strain is increased (Figure 6d), bending and reorientation of sections cause the number of highly stressed sections to increase. This eventually leads to the formation of an oriented axial stress path, i.e. filament sections that percolate through the network (appearing in thick red in Figure 6d,e). Once the stress path is formed, further shearing mainly increases the axial stress of the sections in the path, while the path itself extends and straightens (Figure 6d,e). The increase

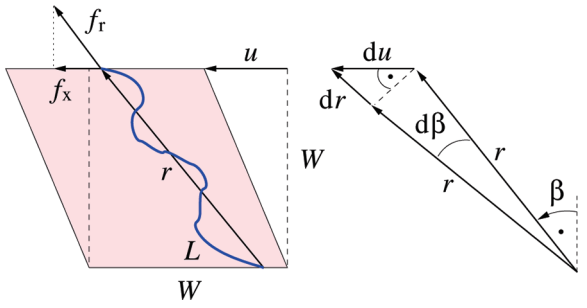

Figure 7. Simple shear of a box containing a single filament.

of the axial stress in these sections emerges as the dominant load carrying part of the network (Figure 6e). Therefore, while it is the collective bending of filament sections that is responsible for the linear network response at small strains, the network stiffening and the transition to the 3/2 power law region are caused by the localized formation and stretching of undulated paths comprising highly axially loaded sections. The stress paths in networks of relatively low connectivity are commonly found as a single percolation (see Figure 6d,e), while for networks of higher connectivity several interconnected stress paths may form a supportive frame. The concept of a supportive network frame that emerges with shearing of the network has also been observed by Kim et al. in MD simulations of actin networks.[28] In agreement with Figure 6b, the pulling-out of the stress path undulations is a process dominated by the bending energy. The axial energy becomes significant only at very high stress where rupture of the filaments is expected. The torsional energy contributes only up to ≈15% in the small strain linear regime; as soon as the network starts to stiffen with the 3/2 power law, the torsional energy begins to vanish.

Since the percolating stress path dominates the overall stress response, it can be considered alone and isolated from the rest of the network. For networks of lower connectivity where the stress path is just a single percolation through the network, the stress path is a static undulated filament. The straightening-out of a stress path therefore, is mechanically equivalent to the stretching of an undulated athermal filament which has been shown[29] to exhibit the same asymptotic behavior as a thermally undulating filament.[11,12] This observation allows for the following simple model that captures the 3/2 power-law scaling noted above in Figure 5.

Consider a single, athermal yet undulated filament through a box of size W^3, as sketched in Figure 7 (it is sufficient to consider the projection of the percolation onto the shear plane). As the box is sheared by a displacement u, the filament stretches, so that at the moment when the macroscopic shear strain is $\Gamma = u/W$ the filament of contour length L with end-to-end distance r is oriented at angle β. The macroscopic shear stress is determined by the component f_x of the pulling force f_r in the direction of shear, i.e. $T = f_x/W^2$. The corresponding shear modulus $G = \partial T/\partial\Gamma$ behaves as $G \propto df_x/du = (df_x/dr)(dr/du)$. From the geometry shown in Figure 7, $dr = du \sin\beta$ and $f_x = f_r \sin\beta$. Typically once the 3/2 power low region sets in (Figure 6d), the network rapidly stiffens so that the change of the filament orientation with shear is very small and the angle β can be considered as constant. For constant β, $df_x = df_r \sin\beta$. Thus, the strain dependence of the macroscopic shear modulus G is mainly governed by the filament response, i.e.

$$G \propto \frac{df_r}{dr} \qquad (6)$$

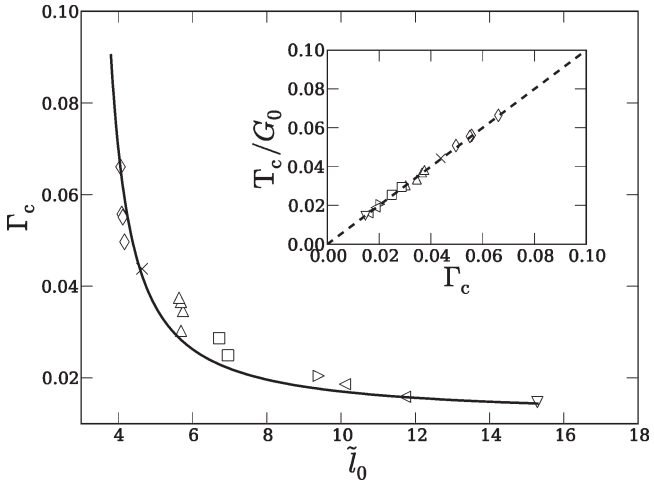

Figure 8. Critical strain Γ_c as a function of $\tilde{l}_0$. The solid line is a fit of the expected scaling according to eq 7 with proportionality constant ≈0.01. Inset: Critical stress scaled by the initial network shear modulus T_c/G_0 as a function of critical strain Γ_c. The dashed line shows the expected dependence $T_c/G_0 = \Gamma_c$. The symbols are the data obtained from the networks in Figure 5.

The excess length stored in filament undulations, or the slack $\mathcal{S}$, is the difference between the filament contour length and its current end-to-end distance, i.e. $\mathcal{S} = L - r$. Since the force f_r in the undulated filament close to its full extension ($\mathcal{S} \to 0$) is diverging with $\mathcal{S}$ according to $f_r \propto 1/\mathcal{S}^2$,[29] in the same manner as in the worm-like chain model, we find that $G \propto 1/\mathcal{S}^3$. In terms of the macroscopic stress T, the shear modulus behaves as $G \propto T^{3/2}$ since $T \propto f_x \propto f_r \propto 1/\mathcal{S}^2$. Thus, from the analogy between percolating network stress paths and undulated filaments, the exponent 3/2 in the stress dependence of the nonlinear network response in Figure 5 originates from the pulling-out of undulations in the nearly extended stress paths and the diverging dependence of the pulling force on the slack.

The existence of a master curve, as shown, e.g., in Figure 5, suggests that T_c and Γ_c are somehow related to connectivity. Since T_c itself is a function of Γ_c by definition, we only have to consider the relationship between the critical strain Γ_c and the connectivity. The critical strains Γ_c for the data sets of Figure 5 are shown in the main graph of Figure 8 as a function of the connectivity parameter $\tilde{l}_0$.

Using the expression eq 5 proposed for the master curve $\tilde{G}(T/T_c)$, we now derive a theoretical scaling for Γ_c versus $\tilde{l}_0$ as follows. First we note that from the linear region of the network response ($\Gamma \le \Gamma_c$), it follows that the shear modulus at the critical point is close to the initial network response, $G/G_0 \approx 1$ and that $T_c = G_0\Gamma_c$. On the other hand, from the functional form of the master curve $\tilde{G}(T/T_c)$ introduced above, the stress dependent shear modulus can be found as $G = G_0 + aG_0/T_c^{3/2}(T - T_c)^{3/2}$. Assuming that $aG_0/T_c^{3/2}$ is independent of connectivity $\tilde{n}_X$ and by using $T_c = G_0\Gamma_c$, the initial shear modulus is thus expected to scale with critical strain as $G_0 \propto \Gamma_c^{-3}$. In Figure 4 it was shown that the normalized shear modulus is only a function of strain and connectivity, $\tilde{G}(\Gamma;\tilde{n}_X)$; therefore, rescaling the strain by Γ_c leads to the master curve $\tilde{G}(\Gamma/\Gamma_c)$. Since the master curve $\tilde{G}(\Gamma/\Gamma_c)$ has to be independent of connectivity $\tilde{n}_X$, the dependence on $\tilde{n}_X$ in $\tilde{G}(\Gamma;\tilde{n}_X)$ has to arise from Γ_c, i.e. Γ_c is a function of connectivity $\tilde{n}_X$ only. Combining $G_0 \propto \tilde{n}_X^{5/2}$ (see Figure 3),

and $G_0 \propto {\Gamma_c}^{-3}$, it follows that $\Gamma_c \propto {\tilde{n}_X}^{-5/6}$. Replacing $\tilde{n}_X$ with $\tilde{n}_X(\tilde{l}_0)$ we expect the following scaling for Γ_c vs $\tilde{l}_0$:

$$\Gamma_c \propto \left(\frac{\tilde{l}_0 - 3}{\tilde{l}_0 - 1}\right)^{-5/3} \quad (7)$$

This trend is indeed captured very well by the numerical data in Figure 8. From the same figure, it can be seen that with increasing network connectivity, Γ_c shifts to smaller values. In the limit of high connectivity $\tilde{l}_0 \rightarrow \infty$, the critical strain Γ_c is bounded from below by the proportionality constant in eq 7 being equal to $\approx$0.01. In addition, the inset of the Figure 8 confirms the expected relation for the critical stress, $T_c = G_0\Gamma_c$. Finally, Figure 8 and the agreement of the data with eq 7 justifies the earlier assumption that $aG_0/{T_c}^{3/2}$ is independent of the network connectivity $\tilde{n}_X$.

5. SUMMARY AND CONCLUSIONS

In this paper, we presented the results of a numerical study on 3D isotropic networks of rigidly cross-linked athermal filaments under shear. It was shown that the topological network properties can be described solely in terms of the ratio of the mean filament and section length $\tilde{l}_0 = l_0/l_c$. The network connectivity, here associated with the fraction of the 4-coordinated cross-links $\tilde{n}_X(\tilde{l}_0)$, strongly modulates the initial shear modulus of networks of low to moderate connectivities, while for networks of very high connectivity the dependence on connectivity weakens and becomes insignificant.

When sheared to large strains, the network exhibits a response with a modulus G that is independent of strain Γ up to the critical point, after which it becomes nonlinear and is characterized by a power law dependence of the network modulus on macroscopic stress as $G \propto T^{3/2}$. The universal nonlinear behavior of the networks was captured by carrying out the appropriate normalization, i.e. G/G_0, Γ/Γ_c and T/T_c. The master curves as well as the exponent 3/2 are in good agreement with the experiments performed on various *in vitro* networks of rigidly cross-linked filaments.[5,10]

Interestingly, the distorting microstructure of the network during deformation revealed that the nonlinear network response is dominated by nearly fully extended percolating paths comprised of axially stressed sections. Contrary to this highly localized phenomena, the linear network response originates from the collective reorientation and bending of all network sections. From the analogy between the stress paths and undulated filaments, the force required to stretch nearly fully extended stress paths is inversely proportional with the square of the stress path slack, which directly explains the exponent 3/2 found for the stiffness scaling.

The critical strain Γ_c is found to be an intrinsic property of the network microstructure and depends on its connectivity. The shift of Γ_c with increasing network connectivity toward smaller values, as shown in Figure 8, qualitatively corresponds to the experimentally observed trend that Γ_c decreases with increasing concentration of cross-linking proteins.[6] This trend is expected, since the consequence of increasing the concentration of the cross-linking proteins is that more cross-links are made per filament because of which the mean section length l_c becomes smaller and the network connectivity higher.

There is a clear similarity between undulations in network stress paths and thermal undulations in that the tensile response of both diverges as the slack is pulled-out; it is this that allows interpretation of the network response in terms of single filament mechanics. However, there is also a distinct physical difference. While thermal undulations arise from the filament interacting with its environment, the slack of the network stress paths emerges purely from the network microstructure.

This emphasizes once again the importance of the network microstructure for the mechanical behavior. The ways in which the microstructure is influencing the network response is found to be key in qualitatively and quantitatively matching many of the experimentally observed trends. Extension of the model presented here to include cross-link compliance promises a valuable tool for future studies of filamentous network mechanics.

■ ASSOCIATED CONTENT

Supporting Information. Master curves $\tilde{G}(\Gamma/\Gamma_c)$ and $\Gamma/\Gamma_c(T/T_c)$. This material is available free of charge via the Internet at http://pubs.acs.org.

■ AUTHOR INFORMATION

Corresponding Author

*E-mail: (G.Z.) G.Zagar@rug.nl; (E.V.d.G.) E.Van.Der.Giessen@rug.nl.

■ REFERENCES

(1) Lodish, H.; Berk, A.; Zipursky, S. L.; Matsudaira, P.; Baltimore, D.; Darnell, J. *Molecular Cell Biology*, 4th ed.; W. H. Freeman and Company: San Francisco, CA, 2000.
(2) Bausch, A. R.; Kroy, K. *Nature Phys.* **2006**, *2*, 231–238.
(3) Lieleg, O.; Claessens, M. M. A. E.; Bausch, A. R. *Soft Matter* **2010**, *6*, 218–225.
(4) Wagner, B.; Tharmann, R.; Haase, I.; Fischer, M.; Bausch, A. R. *Proc. Natl. Acad. Sci. U.S.A.* **2006**, *103*, 13974–13978.
(5) Gardel, M. L.; Shin, J. H.; MacKintosh, F. C.; Mahadevan, L.; Matsudaira, P.; Weitz, D. A. *Science* **2004**, *304*, 1301–1305.
(6) Tharmann, R.; Claessens, M. M. A. E.; Bausch, A. R. *Phys. Rev. Lett.* **2007**, *98*, 088103.
(7) Xu, J.; Tseng, Y.; Wirtz, D. *J. Biol. Chem.* **2000**, *275*, 35886–35892.
(8) Gardel, M. L.; Shin, J. H.; MacKintosh, F. C.; Mahadevan, L.; Matsudaira, P. A.; Weitz, D. A. *Phys. Rev. Lett.* **2004**, *93*, 188102.
(9) Yao, N. Y.; Broedersz, C. P.; Lin, Y.-C.; Kasza, K. E.; MacKintosh, F. C.; Weitz, D. *Biophys. J.* **2010**, *98*, 2147–2153.
(10) Lin, Y.-C.; Yao, N. Y.; Broedersz, C. P.; Herrmann, H.; MacKintosh, F. C.; Weitz, D. A. *Phys. Rev. Lett.* **2010**, *104*, 058101.
(11) MacKintosh, F. C.; Käs, J.; Janmey, P. A. *Phys. Rev. Lett.* **1995**, *75*, 4425.
(12) Storm, C.; Pastore, J. J.; MacKintosh, F. C.; Lubensky, T. C.; Janmey, P. A. *Nature* **2005**, *435*, 191–194.
(13) Hatami-Marbini, H.; Picu, R. C. *Phys. Rev. E* **2008**, *77*, 062103.
(14) Huisman, E. M.; Storm, C.; Barkema, G. T. *Phys. Rev. E* **2008**, *78*, 051801.
(15) Onck, P. R.; Koeman, T.; Van Dillen, T.; Van der Giessen, E. *Phys. Rev. Lett.* **2005**, *95*, 178102.
(16) Huisman, E. M.; Van Dillen, T.; Onck, P. R.; Van der Giessen, E. *Phys. Rev. Lett.* **2007**, *99*, 208103.
(17) Ghosh, A.; Samuel, J.; Sinha, S. *Phys. Rev. E* **2007**, *76*, 061801.
(18) Astrom, J. A.; Kumar, P. B. S.; Vattulainen, I.; Karttunen, M. *Phys. Rev. E* **2008**, *77*, 051913.
(19) Kim, T.; Hwang, W.; Kamm, R. *Exp. Mech.* **2009**, *49*, 91–104.
(20) Schmidt, C. F.; Baermann, M.; Isenberg, G.; Sackmann, E. *Macromolecules* **1989**, *22*, 3638–3649.
(21) Head, D. A.; Levine, A. J.; MacKintosh, F. C. *Phys. Rev. E* **2003**, *68*, 061907.

(22) Buxton, G. A.; Clarke, N. *Phys. Rev. Lett.* **2007**, *98*, 238103.
(23) Satcher, R. L., Jr.; Dewey, C. F., Jr. *Biophys. J.* **1996**, *71*, 109–118.
(24) Gibson, L. J.; Ashby, M. F. *Cellular solids*, 2nd ed.; Cambridge University Press: Cambridge, U.K., 1997.
(25) Žagar, G.; Onck, P. R.; Van der Giessen, E. In *IUTAM Symposium on Cellular, Molecular and Tissue Mechanics*; Garikipati, K., Arruda, E. M., Eds.; 2010; pp 161−169.
(26) Liu, X.; Pollack, G. H. *Biophys. J.* **2002**, *83*, 2705–2715.
(27) Ott, A.; Magnasco, M.; Simon, A.; Libchaber, A. *Phys. Rev. E* **1993**, *48*, R1642.
(28) Kim, T.; Hwang, W.; Lee, H.; Kamm, R. D. *PLoS Comput. Biol.* **2009**, *5*, e1000439.
(29) Van Dillen, T.; Onck, P.; Van der Giessen, E. *J. Mech. Phys. Solids* **2008**, *56*, 2240–2264.